Alam et al. *NPG Asia Materials* (2023) 15:65
https://doi.org/10.1038/s41427-023-00511-x

NPG Asia Materials

ARTICLE Open Access

Swift 4D printing of thermoresponsive shape-memory polymers using vat photopolymerization

Fahad Alam[1], Jabir Ubaid[2], Haider Butt[3] and Nazek El-Atab[1]

Abstract

Shape-memory polymers (SMPs) are smart materials that have gained significant attention in recent years owing to their widespread application in smart structures and devices. Digital light processing (DLP), a vat-photopolymerization-based technique, is a significantly faster technology for printing a complete layer in a single step. The current study reports a facile and fast method for the 3D printing of SMP-based smart structures using a DLP 3D printer and a customized resin. A liquid crystal (LC, RM257) was combined with the resin to introduce shape-memory properties. The combination of LCs in photocurable resin provides the opportunity to directly 3D-print thermoresponsive structures, avoiding the complexity of SMP resin preparation. The structures were printed with different geometries, and the shape-memory response was measured. Lattice structures were fabricated and programmed to obtain tunable mechanical properties. Furthermore, the strain-sensing response was measured to demonstrate the utility of these lattice structures as smart patches for joint-movement sensing. The SMPs can be prepared conveniently and can potentially be used for various applications, such as smart tools, toys, and meta-material sensors.

Introduction

Shape-memory polymers (SMPs) belong to a class of dual-shape smart polymers that can be highly mechanically deformed, and their deformities can be reversed (in the fixation state) in response to environmental parameters[1–3]. SMPs can be reconfigured or recovered to their original shape by applying external stimuli, such as heat, light, electricity, humidity, or pH change[4]. SMP materials also referred to as shape-shifting materials, have attracted considerable interest in recent years owing to their versatility, flexibility over various morphologies, and industrial viability[2,5]. SMPs are emerging materials for various engineering applications, including 2-, 3- and 4-dimensional manufacturing of polymers and composites. The shape-shifting ability of these SMPs is highly relevant for biomedical applications such as foldable and deployable smart structures and implants and wearable electronic and flexible devices[6–9]. Thermo-responsive SPMs are programmable via thermomechanical forces while heated and can be programmed to various temporary shapes (programmed shapes) while the SMPs are in the rubbery state[10]. The programmed temporary shape remains in the transition phase. When the temperature exceeds the nematic–isotropic phase transition temperature (T_{NI}), the materials become elastic. Conversely, when below T_{NI}, the chain formation of the shape-memory material becomes limited, and the material remains in its rigid form, which makes it suitable for fixation in the new programmed geometry. Upon heating above the T_{NI}, the shape of SMPs can switch back to its original (memorized) shape[11]. Furthermore, by controlling the extent of heating and the applied mechanical loading, shape programming can be controlled according to the needed application. Shape switching occurs because of the orientation of the domains in the polymer chains[12]. The reversible switch in a

Correspondence: Nazek El-Atab (nazek.elatab@kaust.edu.sa)
[1]Electrical and Computer Engineering, Computer Electrical Mathematical Science and Engineering Division, King Abdullah University of Science and Technology (KAUST), Thuwal 23955-6900, Saudi Arabia
[2]Department of Nuclear Engineering, Khalifa University of Science and Technology, P.O. Box 127788, Abu Dhabi, United Arab Emirates
Full list of author information is available at the end of the article

semicrystalline network begins with changes in the orientation of the domains.

Liquid crystal elastomers (LCEs) are polymeric networks that exhibit shape changes in response to heat[13]. LCEs are soft, multifunctional materials consisting of an anisotropic molecular order of liquid crystals (domain) in a cross-linked polymer network. The switching of the domain from anisotropic to isotropic orientations is stimulated by temperature changes (above and below T_{NI}), making them suitable for soft robotics applications[14,15]. Taking advantage of the shape-shifting ability of SMPs, numerous new (mechanical and biomedical) applications have been developed, including smart heat-shrinkable devices, smart packaging materials, robotic grippers, smart biomedical sensing patches, smart biomedical stents, structures with tunable mechanical properties, and other smart mechanical tools[16–18].

These SMPs can be easily processed via conventional techniques, such as extrusion, compression, and molding; however, the structures produced are typically simpler in shape[19–21]. Furthermore, the permanent shape enabled by the shape-shifting property is mostly restricted when the structures are developed via conventional processing techniques. Additive manufacturing (AM) technologies, such as 3D printing, have gained tremendous interest because of their capability to produce complex structures in a significantly short period[21–23]. Digital light processing (DLP) is a vat-photopolymerization-based 3D printing technology that enables faster printing[24–29]. In DLP, a complete layer is simultaneously exposed, making it a parallel and fast process[17,18]. Furthermore, the ink materials needed for DLP are easier to develop, and larger amounts can be easily prepared. In addition to less time consumption and the easier process for the development of feedstock materials, compared to extrusion-based 3D printing, DLP 3D printing generates a real 3D structure. DLP 3D printing is capable of 3D printing of complex hierarchal structures with high accuracy at the micro- and macroscopic levels, which is not possible with conventional manufacturing methods. Furthermore, by taking advantage of DLP technology, i.e., photocuring of liquid resin, it is easier to mix any secondary material in it and print the structure. The combination of filler material in photocurable resin provides the opportunity to directly 3D-print stimuli-responsive structures, avoiding the hassle of the complex process of stimuli-responsive resin preparation. The technology of DLP is very simple, and open source (open for customized resin materials) desktop 3D printers are readily available, which makes it possible to customize resin according to a targeted application. In addition, it is easy to print different structures at the same time because in DLP, the whole print bed can be filled with different structures, and they can be printed together. Joint movement sensing via smart patches has been reported by utilizing stretchable patches[30], but individual-specific customization is relatively difficult. The use of SMP-based smart patches allows the advantage of individualized and specific customization.

In the current study, the 4D printing of SMPs was demonstrated via the DLP 3D printing method, which is a vat-photopolymerization-based technique. The SMPs were 4D printed using a DLP 3D printer, and a customized resin was utilized as the crosslinker. Liquid crystals (LCs) were exploited as thermosensitive actuators, helping to introduce the shape-memory response. This study reports an easy and fast method for the 4D printing of SMPs. To introduce the shape-memory property into the material, a liquid crystal (RM257) was combined with an acrylic-based commercial resin to introduce shape-memory properties into the 3D-printed structures. The samples were printed with different geometries, and the shape-morphing response was measured. This study demonstrates the suitability of 3D-printed complex structures for various applications. Metamaterials (lattice structures) were fabricated, and control over the tuning of mechanical properties was demonstrated by programming them in different temporary states. Finite element analysis (FEA) of the lattice structures was performed to study the mechanical properties of the different programmed shapes. Furthermore, smart patches were demonstrated by applying a nanosilver paste coating on 3D-printed lattice structures that behaved as active wearable devices.

Materials and methods

Materials

The liquid crystal (1,4-Bis-[4-(3-acryloyloxypropyloxy) benzoyloxy]-2-methylbenzene ($C_{33}H_{32}O_{10}$) (RM257)) was purchased from Wilshire Technologies and was used as received. A commercial resin (Voxlab, standard transparent) composed of acrylic monomers, a methacrylate oligomer as a crosslinker, and diphenyl (2,4,6-trimethylbenzoyl) phosphine oxide as a photoinitiator was utilized as the photocurable resin. Analytical-grade isopropyl alcohol (Merck, Darmstadt, Germany) was used to clean the 3D-printed specimens.

Preparation of shape-memory polymer resin

To prepare the photocurable shape-memory polymer resin, the liquid crystal RM257 was combined with the commercial resin. First, RM257 (5 wt% of the resin formulation) was dissolved in toluene at 70 °C on a hot plate by continuous stirring. Stirring continued until a transparent solution was obtained. In the next step, the LCs dissolved in toluene were mixed with the commercial resin and continuously stirred using a magnetic stirrer at 70 °C. The mixture was stirred until a homogeneous mixture was obtained. To avoid exposure to ambient light, the flask was covered with aluminum foil. To evaporate

the toluene, the prepared resin solution was kept in an oven at 60 °C overnight. The prepared resin was used for the 3D printing of the samples.

Preparation of CAD model and 3D printing

The 3D models of different geometries of the samples were developed by a computer-aided designing (CAD) tool called SOLIDWORKS© (Dassault Systèmes SOLIDWORKS Corp). CAD models of flat rectangular plates, flower petals, foldable packaging, and lattice structures with different geometries were prepared. The CAD files were generated in stereolithography (.stl) file format and subsequently converted into 3D printer-readable files. The 3D printing process of the samples was performed using a digital light processing (DLP)-based 3D printer (Prusa SL1S). The complete fabrication steps involved in the 3D printing process are shown in Fig. 1. The chemical composition of the resin and liquid crystal utilized is shown in Fig. 1A. PrusaSlicer 2.5.0, a slicing tool from Prusa, was used to slice the model into layers for printing. The process of DLP 3D printing is schematically presented in Fig. 1B, which shows the components of the 3D printer: the light source, resin tray, and print bed. The liquid monomer resin was cured using UV light (wavelength: 405 nm), as indicated in Fig. 1B. After printing, the samples were removed from the print bed and washed with an isopropyl alcohol (IPA) solution to remove any uncured resin. The printing parameters are listed in Table 1. A rectangular plate printed using this method was programmed into another temporary shape (arc), and the shape-shifting is shown in Fig. 1C. The shape-shifting process is schematically depicted in Fig. 1D.

Finite element analysis (FEA)

To simulate the mechanical performance of SMP lattice structures with different programmed states, FEA was performed using a commercial FEA code called ABAQUS (Dassault Systemes). The structures were meshed using 2-node linear beam elements (B31) available in ABAQUS. The elastic and plastic properties of the SMP were

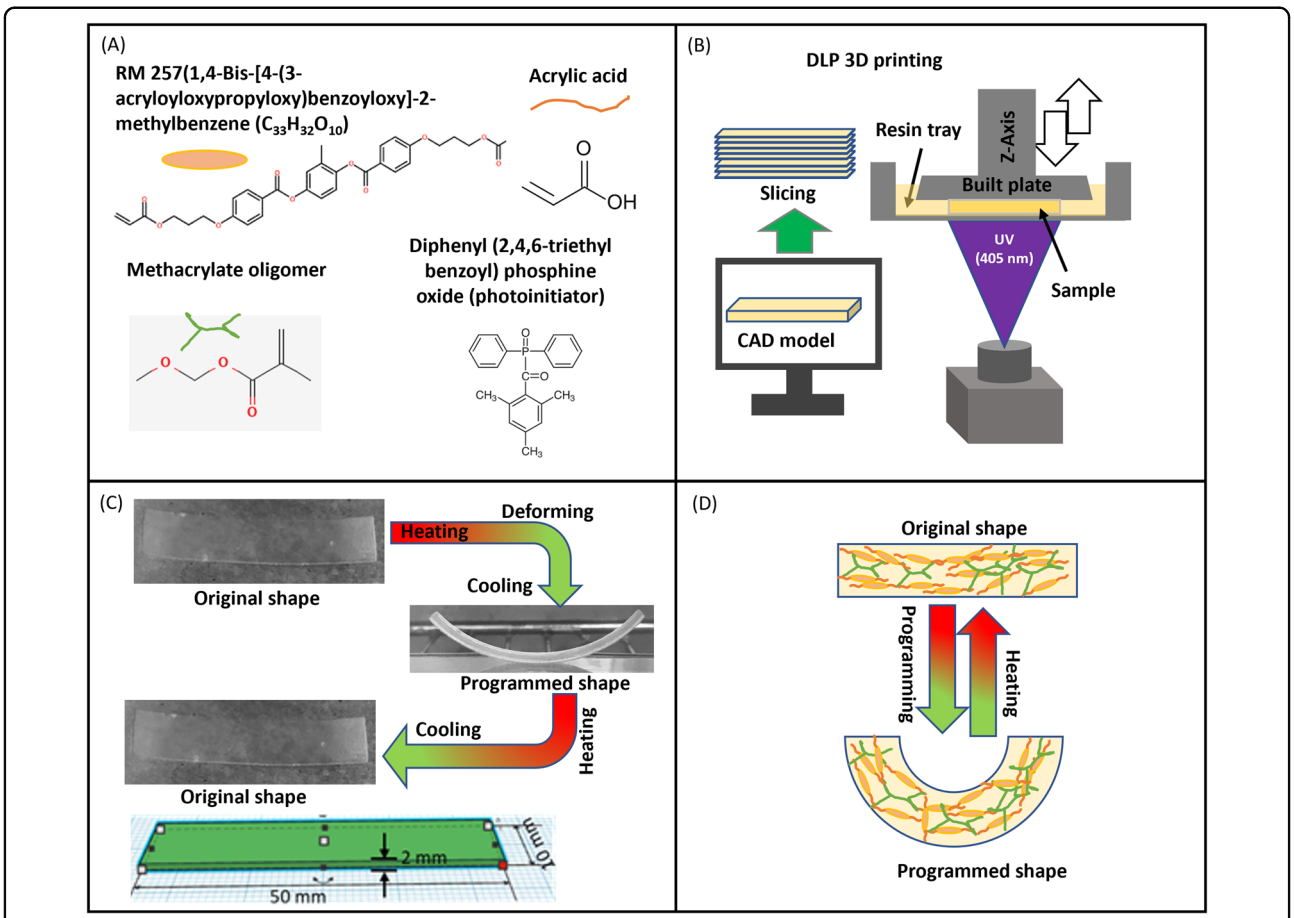

Fig. 1 Digital Light processing specifications. A Schematic illustration of the preparation of a shape-memory polymer by utilizing a liquid crystal (RM257). **B** DLP 3D printing of the prepared shape-memory polymer resin. **C** Digital photographs of the shape-morphing structure. **D** Schematic representation of the programming steps of the 3D-printed sample: (1) heating, (2) cooling, (3) fixing to a new shape, and (4) reheating to regain the original shape.

Table 1 Digital Light Processing (DLP) specifications.

Printing parameters	Value
Layer thickness	25 µm
Curing time	Burn in layers, 25 s; normal layers, 5 s
Speed (normal layers)	Lifting speed, 40 mm/min; lowering speed, 80 mm/min
Speed (slow selection layers)	Lifting speed, 25 mm/min; lowering speed, 40 mm/min
Wait after lift	1 s
Lift height	6 mm (moving up the build plate for 1 s after every layer to separate printed layers from tray)
Support	No support

DLP 3D printing parameters for manufacturing specimens.

obtained from quasistatic uniaxial tensile tests performed according to ASTM D638[31,32] and are listed in Table S1. The ductile damage model available in ABAQUS was used to model material failure; a failure strain of 0.1 at a stress triaxiality of 0.33, which was obtained from the stress–strain response of the tensile samples, was used. Element deletion was utilized in the FE model to remove elements that satisfied the material failure criteria.

Characterization

The shape-memory response of the 3D-printed samples was characterized by programming the samples into a second temporary shape by heating, deformation, and fixation. Shape programming was performed by passing the samples through four steps: heating, mechanical loading, simultaneous holding and cooling, and finally, unloading. The samples were immersed in hot water at 80 °C and deformed while dipped in water for 10 s. Please note that 80 °C was chosen based on previously reported literature[33]. Subsequently, the samples were moved to room temperature conditions and immediately subjected to a load and held for 60 s; this process was performed while in the deformed state. Finally, the samples were left unloaded. By doing this, the samples were fixed in a deformed state, resulting in a second temporary shape. To demonstrate the activation of SMPs, lattice structures (metamaterials)[34] and smart structures were prepared, deformed, and fixed into new shapes. To confirm the actions of SMPs, the deformed samples were reimmersed in hot water and quickly recovered their original shape. Deformation and shape recovery were performed multiple times to demonstrate the repeatability of the SMPs. To examine the internal morphologies of the samples with and without LCs, the samples were observed using scanning electron microscopy (SEM). Micrographs of the specimen cross-sections were observed at different magnifications. Furthermore, the load-bearing capacity was measured to demonstrate the stability of the temporary morphed shape. A 60-g load was applied to the programmed flower-shaped sample of 1.6 g, and images were captured. The loaded sample was exposed to heat to recover its original shape (see the video attached in the Supporting Information).

In this study, by taking advantage of temperature-controlled shape programming, the lattice structure was subjected to different mechanical loading conditions (compression and elongation), leading to mechanically tunable smart structures. To achieve mechanical tunability, the printed lattice structure was elongated and fixed in one case but compressed and fixed in another case. The mechanical properties of the 3D-printed lattice structures and dog-bone samples were measured using quasistatic uniaxial tensile tests. A uniaxial tensile machine (UTM) from Zwick-Roell Z005 fitted with a 2.5-kN load cell at a constant crosshead speed of 1 mm/min and at ambient temperature (~25 °C) was utilized. The elastic modulus, yield strength, ultimate tensile strength, and strain at failure were calculated using the obtained data. The load–displacement plots obtained from the tensile tests were used to derive the stress–strain curves. The stress was calculated from the cross-sectional area, and the gauge length was used to calculate the strain at each point.

Results and discussion

The shape-memory effect of the 3D-printed samples was investigated by the shape programming and recovery process. The results from the three different stages are shown in Fig. 2. To demonstrate the applicability of the developed SMPs and the capability of the 3D printing process, several shapes were printed (Fig. 2A, B), all of which exhibited a shape-memory effect. The CAD models shown in Fig. 1A, B were prepared using a commercial CAD tool. The 3D-printed samples were rigid below T_{NI}; conversely, they became elastomeric above T_{NI}, which allowed us to reshape them into other shapes and fix them to the new shape by lowering the temperature below T_{NI} and holding them in the deformed state. The shapes were reversed to their original form by heating above T_{NI}. Several geometries, that is, lattice structures, wrenches, unicorn toys, and KAUST_SAMA names, were printed and applied to multiple cycles of shape shifting and recovery to test the SMP 3D printing technique. The results showed that this technology allows easy and high-resolution printing of intricate 3D designs, which is not possible with conventional methods. 3D-printed SMP objects can be employed for various applications, such as flexible smart patches, size-variable mechanical tools (wrenches), and deformable toys. Videos showing the shape-memory effect of all objects are presented in the Supporting Information (SV1–7).

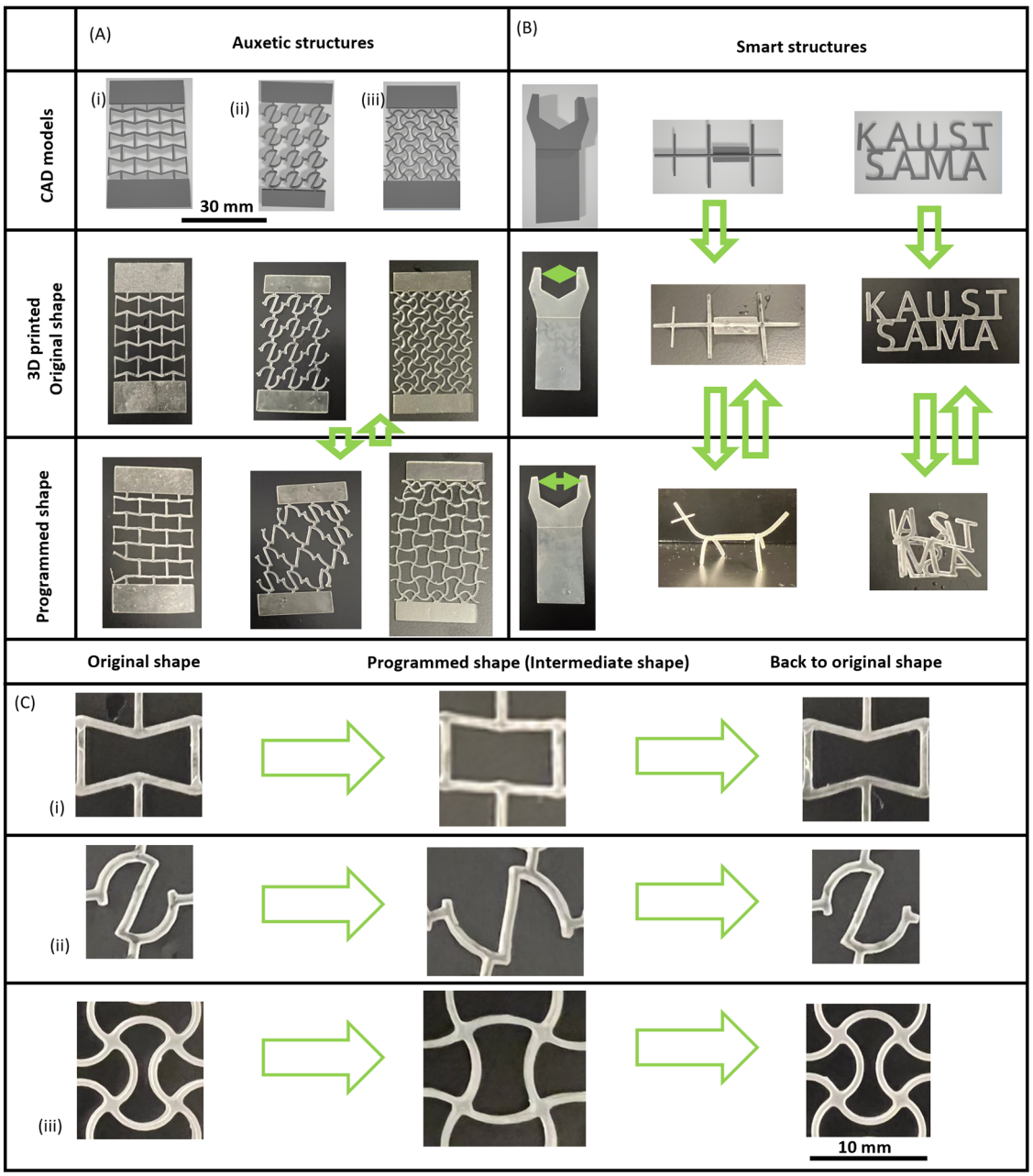

Fig. 2 Programming and recovery of the SMPs (lattice and smart structures). A CAD-model-printed original and programmed shapes of lattice structures: (i) re-entrant lattice, (i) S-shape lattice, and (iii) tetrachiral lattice structures. **B** CAD-model-printed original and programmed shapes of smart structures: (i) size changeable wrench, (i) foldable toy, and (iii) KAUST-SAMA laboratory-printed name (deformed and original). **C** Unit cells of the lattice structure as printed while programming fixed and recovered states.

The shape-memory polymers used in this study were based on a liquid crystal (RM257) mixed with a photo-curable polymer resin, resulting in a semicrystalline polymer. By using a cross-linkable photopolymer and adding the liquid crystal to it, a shape-memory segment and a controllable melt viscosity were created, enabling the shape-memory effect in the resulting polymer. The unit cells of the lattice structure (as printed) while programming fixed and recovered states are presented in the form of digital photos in Fig. 2C. Differences in the shape and size of the unit cells in the original and deformed or programmed shapes can be observed. The arms of the unit cells were pulled for enlargement while being subjected to heat and fixed by holding and cooling, as shown in Fig. 2C (i–iii). To regain the original shape, the fixed or programmed shapes were reheated, and the

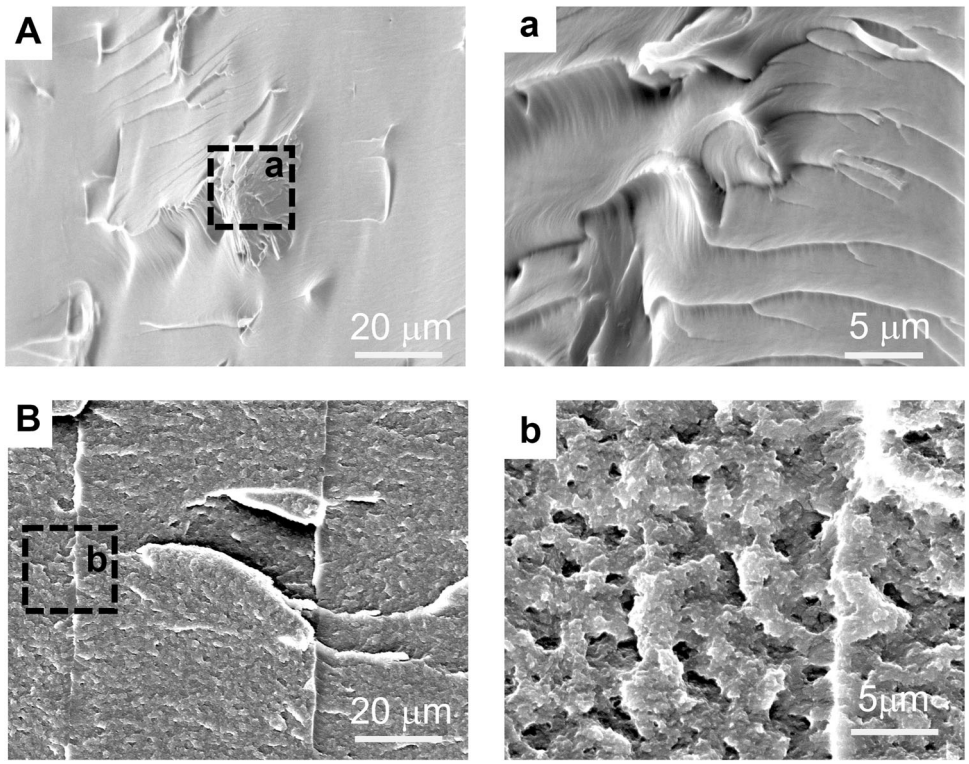

Fig. 3 Micrographs of the cross-section of 3D-printed samples observed under SEM. A Resin only and **B** LC mixed with resin. (a) and (b) are the magnified positions of the micrographs highlighted with dotted yellow lines from (**A**) and (**B**), respectively.

original 3D-printed shapes were automatically recovered, as shown in Fig. 2C (i–iii). The mechanism responsible for the shape-memory effect is depicted based on prior studies available in the literature[27]. The liquid crystals are randomly arranged in the liquid resin, which is then 3D-printed. The layer is cured where the LCs are arranged linearly and cross-linked by oligomers. The mechanism is shown schematically in Fig. SI2. The 3D-printed samples were rigid below T_{NI} (mostly due to the linear arrangement of LCs); conversely, they became elastomeric above T_{NI} (slight bending of LCs). This allowed the samples to reshape into a secondary shape and form a new shape by lowering the temperature below T_{NI}, which held them in a deformed state. The shapes can regain their original form by heating above T_{NI}.

To observe the internal morphology, the cross sections of the 3D-printed samples, with and without LCs, were observed using scanning electron microscopy (SEM), and the results are shown in Fig. 3. Clear differences were observed in the internal morphologies. A smooth surface morphology was observed from the cross-sectioned surface of the sample without LC (Fig. 3A), whereas a rough surface indicated the presence of uniformly distributed LCs in the parent matrix of the LC-mixed sample (Fig. 3B).

Figure 4 shows the shape-memory responses, that is, the programming and recovery of the 3D-printed structures and the load-bearing capacity of the programmed structure. Figure 4A shows the smart foldable box printed in flat form and folded into a box while programming the new box shape, which retained its shape until the heat was applied. Similarly, a shape-memory polymer in a smart packaging morphing structure (Fig. 4B) was printed. One potential application of shape memory is the development of smart optical fibers, as demonstrated in Fig. 4C, which shows the deformation and recovery states of 3D-printed optical fibers. To demonstrate the load-bearing capacity of the programmed flower-shaped 3D-printed structure, the programmed structure was subjected to a 60-g load. The results showed that the structure could bear 50 times its own weight (1.2 g), as shown in Fig. 4D. Furthermore because the current study demonstrates the utility of DLP 3D printing technology in fabricating shape-memory polymers, 3D structures, stents, and ball-shaped structures were printed; the 4D effect is demonstrated in Fig. 4E. The figure shows that the current method is suitable for 3D printing of structures of various shapes and sizes enabled with 4D effects. The quantification of the shape-memory response was performed by the programming and recovery of the 3D-printed U-shaped (shape 1) and flat rectangular (shape 2) discs, and the recovery angle with time (s) was measured. The recovery was much faster in the first case, where the U-shaped structure was made

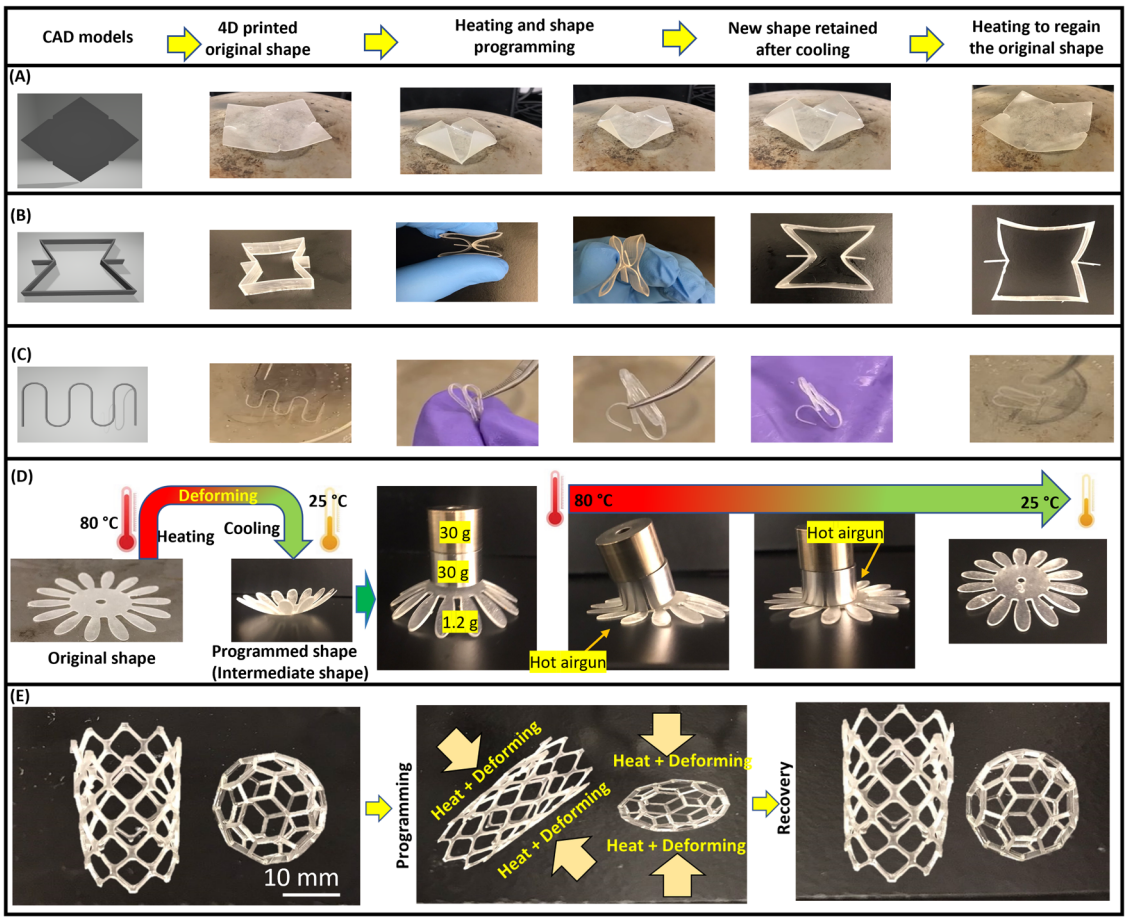

Fig. 4 Programming and recovery of the 3D-printed structures and the load-bearing capacity of the programmed structure. A Foldable box. **B** Smart packaging morphing structure. **C** Deformation and recovery states of 3D-printed fiber. **D** Load-bearing capacity of the programmed flower-shaped 3D-printed structure. **E** Fabrication of 3D structure showing the suitability of the method in printing 2D and 3D structures.

flat, and it recovered into its original shape in 58 s; on the other hand, the recovery was slower in the flat printed and bent to a U-shaped structure (Fig. SI1). It took almost 2 min (122 s) to recover a flat shape from the programmed U-shape. The actual videos are presented in supplementary information SV9 and SV10. To analyze the shape-memory effect, the recovery angle ratio (R_r) was calculated using the equation below[35]:

$$R_r = \frac{(\theta_r - \theta_f)}{180 - \theta_f} \times 100$$

where θ_r and θ_f are the recovery angle and fixed angle, respectively.

Figure 5A shows the recovery angle versus time for both shapes, whereas Fig. 5B shows the recovery angle ratio versus time. Clearly, the recovery rate is faster in shape 1 than in shape 2. Representative photographs of the shape recovery of shapes 1 and 2 are presented in Fig. 5C, D, respectively.

One promising application of 3D-printed SMPs, that is, the tunable mechanical properties[36] of 3D-printed structures, is demonstrated in Fig. 6. The tensile tests were performed on a dog-bone specimen and an as-printed lattice structure, and the results are presented in Fig. 6A, B, respectively. The results indicated that the mechanical properties of 3D-printed structures could be tailored. The 3D-printed lattice structures were programmed to two different states such that they attained different strain conditions: first, the structure was fixed in a stretched state, and second, the structure was fixed in a compressed state (Fig. 6C, inset). The resulting stress–strain plots are shown in Fig. 6C. The mechanical properties calculated from these plots are presented in Table 2. Figure 5c illustrates that the sample programmed into a stretched state displays greater alignment among its members in the loading direction in comparison to the sample programmed into a compressed state, where member alignment in the loading direction is reduced. Consequently, the stretched-state sample primarily undergoes deformation dominated by

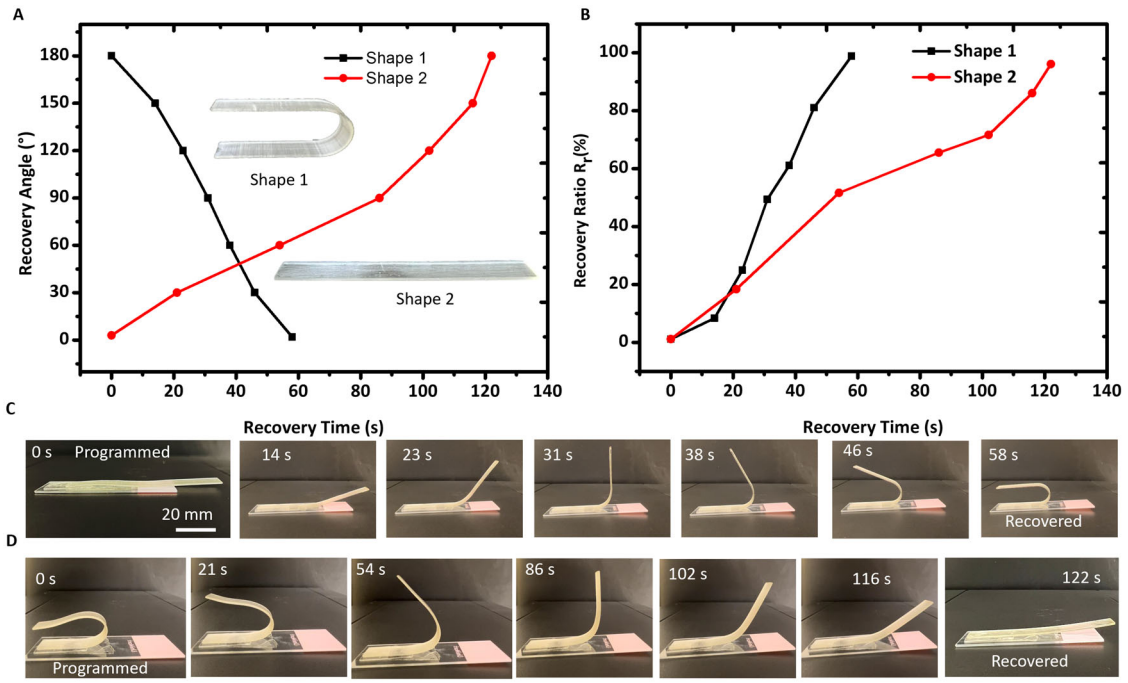

Fig. 5 Shows the quantification of the shape memory effect from the two 3D-printed shapes. A Recovery angle of the shapes with respect to time, **B** recovery ratio of the shapes with respect to time, and **C** digital photographs of the programmed shape while recovering taken at different times (s) until full recovery.

stretching, while the compressed-state sample predominantly exhibits behavior dominated by bending. Because of the prevalence of stretch-dominated behavior, the stretched-state samples exhibited the highest modulus. Conversely, owing to the dominance of bending behavior, the compressed-state samples displayed a lower modulus but demonstrated greater strain-to-failure, strength, and toughness. The results of the mechanical tests of the as-printed and programmed samples suggest that the mechanical properties can be tuned by controlling the shape programming of the lattice structures.

To confirm the mechanical tunability of the SMP structures, FE simulations were performed, and the experimental results from the tensile tests were compared with the results (Fig. 6C) from the FEM analysis. Additionally, images depicting lattice structures in both unloaded and loaded states are presented in Fig. 6E, F, respectively. The mechanical performances of the 2D lattices observed experimentally and predicted by FEA were in reasonable agreement and showed similar trends among the samples. This suggests the possibility of estimating the extent of shape programming needed for the controlled tuning of the mechanical properties using FEA. The difference in the magnitude of the experimental and FEA results is mainly because the structure is in perfect condition in the FEA; however, in reality, the 3D-printed structure contains defects, such as pores, edges, and surface defects. The stability of the programmed shape was measured by performing the tensile test in a cyclic fashion, and the stress–strain curves are plotted in Fig. 6D. The results of the cyclic tensile test suggest that the programmed shapes are stable and retain their tuned mechanical properties. There is a slight decrease in the stress–strain curve after every cycle due to the relaxation of the polymer chain[37], which can be restored by applying heat to its original state. To check long-term stability, cyclic tests were performed for up to 100 cycles. This suggests that the programmed tuning is not perfectly stable, but when load scans were applied multiple times, a clear difference between all three programmed shapes existed, although they started to recover to some extent.

Considering the flexibility and stretchability of the 3D-printed lattice patch, the samples were tested for strain sensing, which is relevant for joint-movement sensing applications. A nanosilver-based conductive coating was applied to the surface of the 3D-printed lattice patch, which acted as an electrode. Alternatively, a conductive composite instead of a conductive silver paste can be used. However, we observed that adding the conductive material to the resin to create a conductive composite for 3D printing requires further optimization of the printing parameters. Changes in electrical resistance were measured while the structure was stretched and compressed. The patch was fixed to the joints, as shown in Fig. 7, and

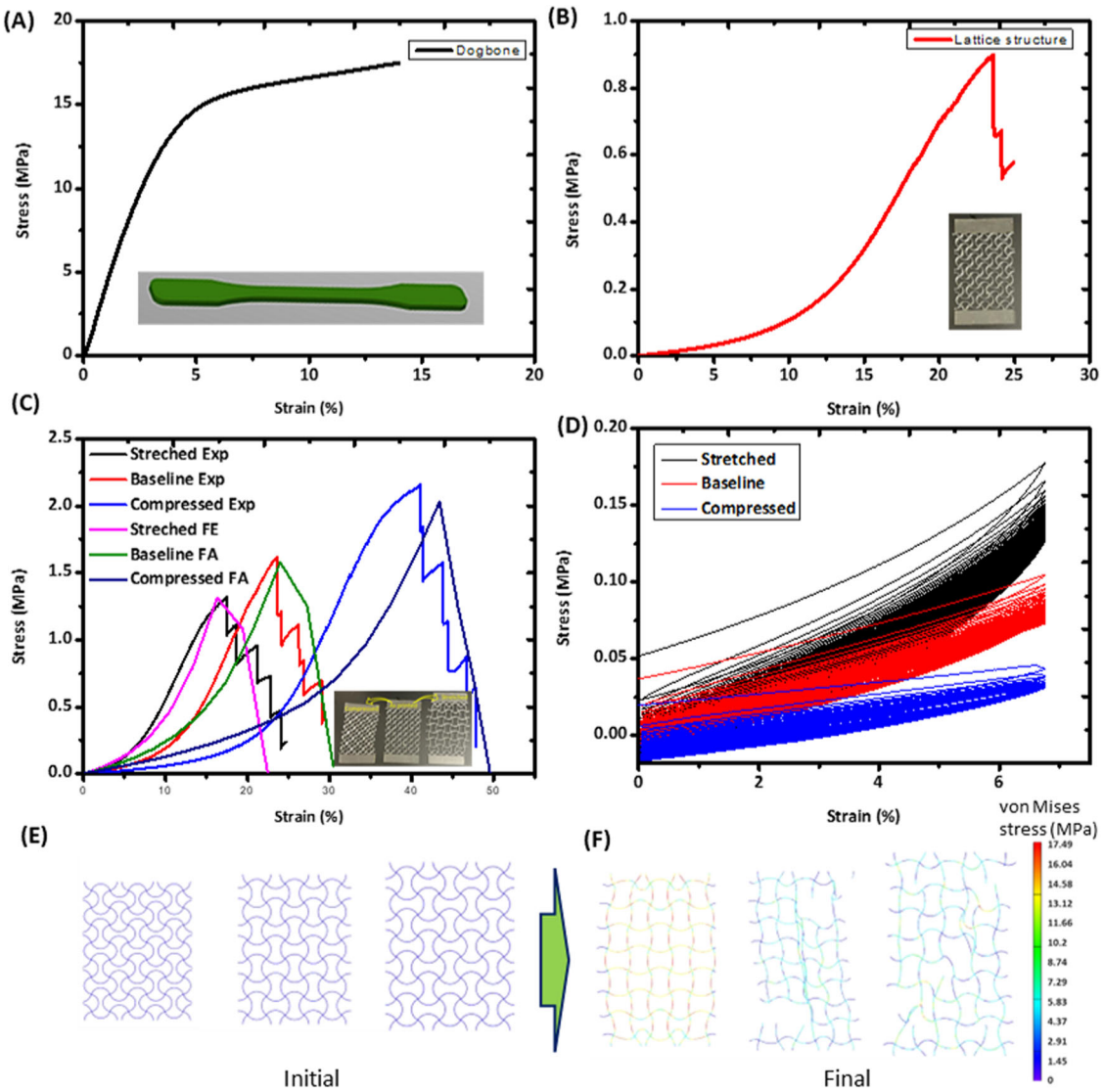

Fig. 6 Tunable mechanical properties of the lattice structures. A Stress–strain plot of the dog-bone specimen under tensile loading. **B** Stress–strain plot of the lattice structures under tensile loading. **C** Experimental stress–strain plots of lattice structures with tuned mechanical properties. **D** Stress–strain plots of lattice structures with tuned mechanical properties obtained from FEA. **E** Stress–strain plots obtained from the cyclic test of the lattice structures with mechanically tuned mechanical properties. **F** FE analysis results showing the initial and final deformation states of the structures and stress distribution in the lattice structures.

Table 2 Mechanical properties of the as-printed and programmed lattice structures.

Samples	Modulus (MPa)	Toughness	Strain at failure	Strength (MPa)
Stretched	1.43 ± 0.05	0.065 ± 0.002	0.17 ± 0.01	0.73 ± 0.03
Baseline	0.76 ± 0.06	0.075 ± 0.008	0.24 ± 0.02	0.89 ± 0.09
Compressed	0.42 ± 0.05	0.157 ± 0.035	0.41 ± 0.09	1.13 ± 0.27

the changes in resistance were measured as a function of time while opening (compressing) and closing (stretching) the joints. As the joint closed, the patch was stretched. This resulted in the separation of silver-coated particles, in which they moved apart from each other (as observed in the SEM images), leading to a longer travel path for electrons. This is depicted in the schematic in Fig. 7C. Conversely when the joint was opened, the patch was compressed, leading to the movement of silver particles closer to each other and leaving a shorter travel path for

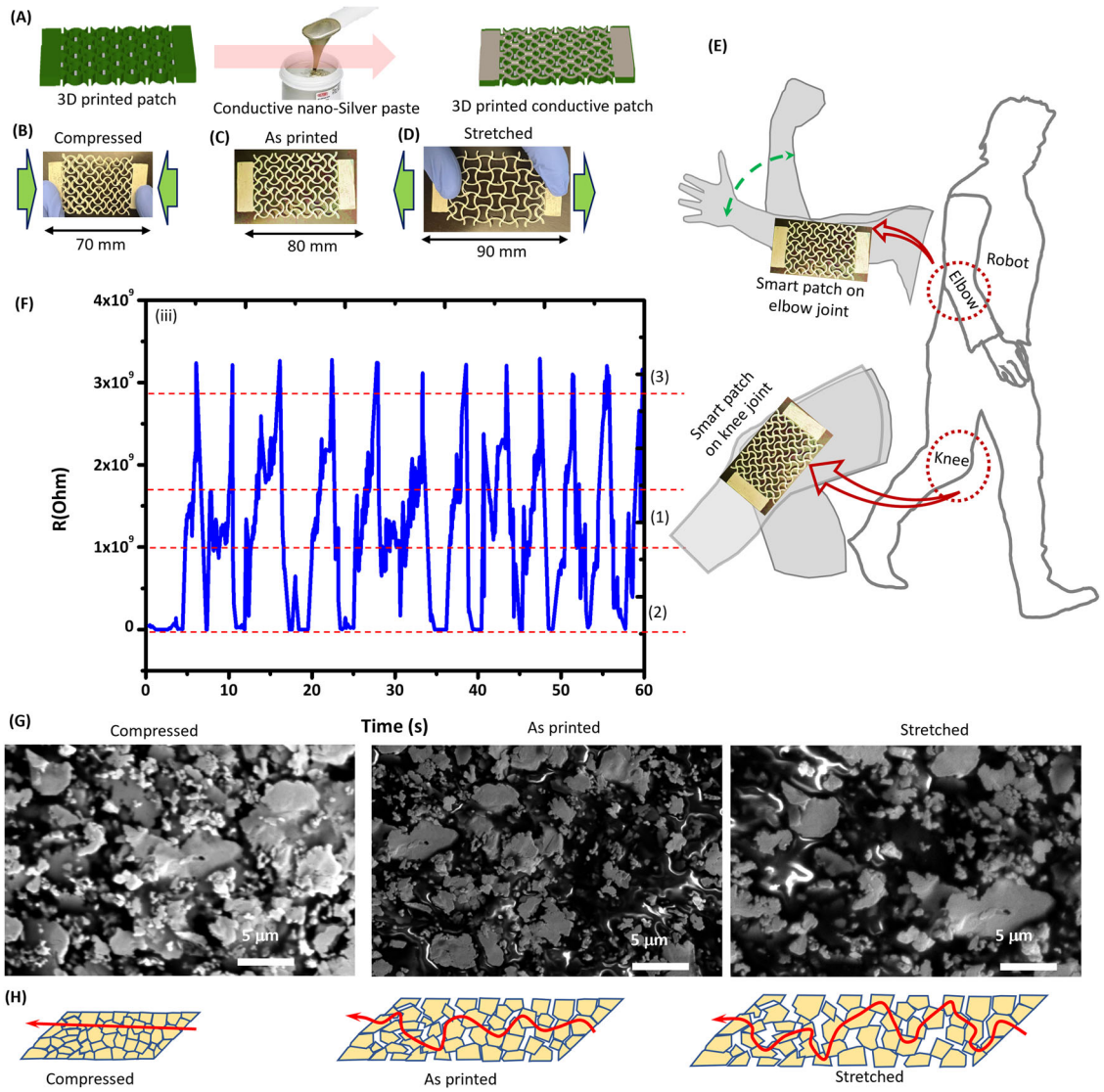

Fig. 7 Application of the smart structure for the joint-movement sensing application. A 3D printing and electrode preparation on a smart lattice patch. Digital photographs of the smart lattice patch in different states: **B** compressed, **C** as-printed and **D** stretched. **E** Application of the smart patch on knee and elbow joints for the bending sensor. **F** Sensing response as a function of change in resistance while bending and straightening the joints. The SEM micrographs from the surface of **G** are shown in the lower portion of the figure, indicated with arrows. **H** The change in the resistance is depicted using a schematic showing the changes in the nanosilver coating microstructure, which resulted from stretching and compression. This change in nanosilver coating changes the path length of the electrons, and their movement is shown using red lines.

electrons. This is shown by the red arrow in Fig. 7A–C. The closer the silver particles are to each other, the shorter the travel path and the lower the resistance, as observed in plot (2). Conversely, the farther the silver particles are from each other, the longer the travel path and the higher the resistance, as observed in plot (3). The test was performed multiple times by opening and closing the joints at a fixed time interval of 5 s, and the resistance change plot is presented in Fig. 7(iii). A similar phenomenon was reported by Cho et al.[38], who observed the effect of crack orientation on the current flow of two different kinds of coatings.

The results from the resistance measurement of the prepared lattice electrode patch showed that it can be used as a smart patch for joint-movement sensing. The prepared smart patch can be applied to a human knee, elbow joints, artificial limb joints or robotic arms, or real limb joints to sense movements. The advantage of using a lattice smart patch prepared from SMPs is the capability of programming the patch according to the size of the patient or robot. Furthermore, the use of DLP printing techniques to prepare smart lattice patches is easier and faster than other manufacturing approaches.

Conclusions

The current study presents a method for 3D printing of smart materials using shape-memory polymers, which allows for easier and faster manufacturing via digital light processing. These 3D-printed objects can be programmed to create structures that change over time, known as 4D structures. To achieve this, a liquid crystal was combined with a resin and was printed using a commercial desktop 3D printer. Various complex objects were successfully created, such as lattice patches, foldable toys, smart packaging, and mechanical wrenches. By subjecting these objects to heat, their shapes could be temporarily changed and then recovered upon subsequent heating. The idea of mechanical tuning was demonstrated by stretching or compressing lattice structures created through 3D printing. Tensile tests showed that the mechanical properties of these structures can be adjusted through shape programming to meet specific application requirements. Additionally, the 3D-printed lattice patches were tested for strain sensing in joint-movement applications. Changes in electrical resistance were recorded from the 3D-printed smart patch as the joint opened and closed, allowing its application as a smart patch for movement detection in artificial limb joints or robotic arms.

Acknowledgements
This study was supported by King Abdullah University of Science and Technology through the baseline fund.

Author details
[1]Electrical and Computer Engineering, Computer Electrical Mathematical Science and Engineering Division, King Abdullah University of Science and Technology (KAUST), Thuwal 23955-6900, Saudi Arabia. [2]Department of Nuclear Engineering, Khalifa University of Science and Technology, P.O. Box 127788, Abu Dhabi, United Arab Emirates. [3]Department of Mechanical Engineering, Khalifa University of Science and Technology, P.O. Box 127788, Abu Dhabi, United Arab Emirates

Author contributions
FA designed and conducted the experiments, and wrote the manuscript, JU helped in conducting FE analysis and wrote the manuscript, HB helped in proofreading the manuscript and NEA conceived the idea, supervised the experimental and manuscript writing parts, and secured funds for the project.

Conflict of interest
The authors declare no competing interests.

Supplementary information The online version contains supplementary material available at https://doi.org/10.1038/s41427-023-00511-x.

Received: 20 June 2023 Revised: 8 October 2023 Accepted: 17 October 2023.
Published online: 15 December 2023

References

1. Delaey, J., Dubruel, P. & Van Vlierberghe, S. Shape-memory polymers for biomedical applications. *Adv. Funct. Mater.* **30**, 1909047 (2020).
2. Xia, Y., He, Y., Zhang, F., Liu, Y. & Leng, J. A review of shape memory polymers and composites: mechanisms, materials, and applications. *Adv. Mater.* **33**, 2000713 (2021).
3. Zhang, B. et al. Mechanically robust and UV-curable shape-memory polymers for digital light processing based 4D printing. *Adv. Mater.* **33**, 2101298 (2021).
4. Dutta, S. & Cohn, D. Temperature and pH responsive 3D printed scaffolds. *J. Mater. Chem. B* **5**, 9514–9521 (2017).
5. Cheng, C.-Y. et al. 4D printing of shape memory aliphatic copolyester via UV-assisted FDM strategy for medical protective devices. *Chem. Eng. J.* **396**, 125242 (2020).
6. Imrie, P. & Jin, J. Polymer 4D printing: advanced shape-change and beyond. *J. Polym. Sci.* **60**, 149–174 (2022).
7. Haleem, A., Javaid, M., Singh, R. P. & Suman, R. Significant roles of 4D printing using smart materials in the field of manufacturing. *Adv. Ind. Eng. Polym. Res.* **4**, 301–311 (2021).
8. Huang, X. et al. Tracing evolutions in electro-activated shape memory polymer composites with 4D printing strategies: a systematic review. *Compos. Part A: Appl. Sci. Manuf.* **147**, 106444 (2021).
9. Manikandan, N., Rajesh, P. K. & Harish, V. An analysis of the methods and materials for 4-dimensional printing. *Mater. Today.: Proc.* **38**, 2167–2173 (2021).
10. Falahati, M. et al. Smart polymers and nanocomposites for 3D and 4D printing. *Mater. Today* **40**, 215–245 (2020).
11. Kong, D. & Xiao, X. J. S. R. High cycle-life shape memory polymer at high temperature. *Sci. Rep.* **6**, 1–10. (2016).
12. Zhao, Q., Qi, H. J. & Xie, T. Recent progress in shape memory polymer: new behavior, enabling materials, and mechanistic understanding. *Prog. Polym. Sci.* **49-50**, 79–120 (2015).
13. Ambulo, C. P. et al. Processing advances in liquid crystal elastomers provide a path to biomedical applications. *J. Appl. Phys.* **128**, 140901 (2020).
14. Wang, Y. et al. Emerging 4D printing strategies for next-generation tissue regeneration and medical devices. *Adv. Mater.* **34**, 2109198 (2022).
15. Javed, M. et al. Programmable shape change in semicrystalline liquid crystal elastomers. *ACS Appl. Mater. Interfaces* **14**, 35087–35096 (2022).
16. Zomer, R. J. et al. Global tree cover and biomass carbon on agricultural land: the contribution of agroforestry to global and national carbon budgets. *Sci. Rep.* **6**, 29987 (2016).
17. Peng, B., Yang, Y., Ju, T. & Cavicchi, K. A. Fused filament fabrication 4D printing of a highly extensible, self-healing, shape memory elastomer based on thermoplastic polymer blends. *ACS Appl. Mater. Interfaces* **13**, 12777–12788 (2021).
18. Deng, M. et al. Wearable fluorescent contact lenses for monitoring glucose via a smartphone. *Sens. Actuators B: Chem.* **352**, 131067 (2022).
19. Razzaq, M. Y. et al. 4D Printing of multicomponent shape-memory polymer formulations. *Appl. Sci.* **12**, 7880 (2022).
20. Ali, M. H., Abilgaziyev, A. & Adair, D. 4D printing: a critical review of current developments, and future prospects. *Int. J. Adv. Manuf. Technol.* **105**, 701–717 (2019).
21. Ikram, H., Al Rashid, A. & Koç, M. Additive manufacturing of smart polymeric composites: literature review and future perspectives. *Polym. Compos.* **43**, 6355–6380 (2022).
22. Huang, Z., Shao, G. & Li, L. Micro/nano functional devices fabricated by additive manufacturing. *Prog. Mater. Sci.* **131**, 101020 (2023).
23. Yaragatti, N. & Patnaik, A. A review on additive manufacturing of polymers composites. *Mater. Today.: Proc.* **44**, 4150–4157 (2021).
24. Huang, L. et al. Ultrafast digital printing toward 4D shape changing materials. *Adv. Mater.* **29**, 1605390 (2017).
25. Joharji, L. et al. 4D printing: a detailed review of materials, techniques, and applications. *Microelectron. Eng.* **265**, 111874 (2022).
26. Alam, F. et al. Prospects for additive manufacturing in contact lens devices. *Adv. Eng. Mater.* **23**, 2000941 (2021).
27. Li, S. et al. Digital light processing of liquid crystal elastomers for self-sensing artificial muscles. *Sci. Adv.* **7**, eabg3677 (2021).
28. Tang, T., Alfarhan, S., Jin, K. & Li, X. 4D Printing of seed capsule-inspired hygro-responsive structures via liquid crystal templating-assisted vat photopolymerization. *Adv. Funct. Mater.* **33**, 2211602 (2023).
29. Traugutt, N. A. et al. Liquid-crystal-elastomer-based dissipative structures by digital light processing 3D printing. *Adv. Mater.* **32**, 2000797 (2020).
30. Zhao, K., Niu, W. & Zhang, S. Highly stretchable, breathable and negative resistance variation textile strain sensor with excellent mechanical stability for wearable electronics. *J. Mater. Sci.* **55**, 2439–2453 (2020).
31. Alam, F., Varadarajan, K. M., Koo, J. H., Wardle, B. L. & Kumar, S. Additively manufactured polyetheretherketone (PEEK) with carbon nanostructure

reinforcement for biomedical structural applications. *Adv. Eng. Mater.* **22**, 2000483 (2020).
32. D638 A. *American Society for Testing and Materials*, Vol. 82, 1. (ASTM International, 2016).
33. Spiegel, C. A., Hackner, M., Bothe, V. P., Spatz, J. P. & Blasco, E. 4D Printing of shape memory polymers: from macro to micro. *Adv. Funct. Mater.* **32**, 2110580 (2022).
34. Greaves, G. N., Greer, A. L., Lakes, R. S. & Rouxel, T. Poisson's ratio and modern materials. *Nat. Mater.* **10**, 823–837 (2011).
35. Shan, W., Chen, Y., Hu, M., Qin, S. & Liu, P. 4D printing of shape memory polymer via liquid crystal display (LCD) stereolithographic 3D printing. *Mater. Res. Express* **7**, 105305 (2020).
36. Peng, X. et al. 4D Printing of freestanding liquid crystal elastomers via hybrid additive manufacturing. *Adv. Mater.* **34**, 2204890 (2022).
37. Arzhakov M. *Relaxation in Physical and Mechanical Behavior of Polymers* 1st edn (CRC Press, 2019).
38. Cho, C. et al. Strain-resilient electrical functionality in thin-film metal electrodes using two-dimensional interlayers. *Nat. Electron.* **4**, 126–133 (2021).